Enhanced and polarized emission from single colloidal CdSe/CdS nanocrystals coupled to a one-dimensional gold grating

F Eloi, H Frederich, F Mazéas, A Kumar, S Buil, Xavier Quélin, A Bouhelier, J-C Weeber, M C Nasilowski, B C Dubertret, et al.

Enhanced and polarized emission from single colloidal CdSe/CdS nanocrystals coupled to a one-dimensional gold grating

F. Eloi,[1] H. Frederich,[1] F. Mazéas,[1] A. Kumar,[2] S. Buil,[1] X. Quélin,[1] A. Bouhelier,[2] J. C. Weeber,[2] M. Nasilowski,[3] B. Dubertret,[3] G. Colas des Francs,[2] and J.-P. Hermier[1,4,*]

[1]*Groupe d'Etude de la Matière Condensée (GEMaC), Université de Versailles-Saint Quentin en Yvelines, CNRS UMR 8635, 45 avenue des Etats-Unis, 78035 Versailles Cedex, France*

[2]*Laboratoire Interdisciplinaire Carnot de Bourgogne (ICB), UMR 6303 CNRS, Université Bourgogne Franche-Comté, 9 Avenue Savary, BP 47870, 21078 Dijon Cedex, France*

[3]*Laboratoire de Physique et d'Étude des Matériaux, CNRS UMR 8213, ESPCI, 10 rue Vauquelin, 75231 Paris, France*

[4]*Institut Universitaire de France, 103 Boulevard Saint-Michel, 75005 Paris, France*

(Received 19 March 2016; revised manuscript received 25 June 2016; published 3 August 2016)

We present in detail the fluorescence properties of single thick-shell CdSe/CdS colloidal nanocrystals coupled to a linear one-dimensional gold grating. In addition to the photoluminescence decay rate increase, we point out that the polarization ratio of the emission is dramatically enhanced. It overcomes 80% and can reach values close to unity. Experimental results are successfully compared to theoretical predictions. Blinking suppression is also reported.

DOI: 10.1103/PhysRevB.94.085301

I. INTRODUCTION

Colloidal core-shell nanocrystals (NCs) are of great research interest due to their wide range of applications and ease of use. Operating at room temperature, these quantum dots can be used for optoelectronic devices [1], biological labeling [2], or as single photon sources [3]. Despite continuous improvements in their synthesis, such as the realization of very thick shells [4,5], these very promising emitters still suffer from residual flickering related to complex phenomena such as their charging and the efficient Auger recombination of the trion [6–8].

At the single molecule level, the NC emission can be controlled by its coupling to plasmonic structures [9–16]. Plasmonic resonances that exhibit broad bandwidths are particularly well suited to enhance the emission of these emitters characterized by a relatively large linewidth at room temperature (∼20 nm [17]). Using this approach, very high Purcell factors can be achieved. Complete suppression of blinking can also be obtained through the acceleration of radiative recombination. Plasmonic structures offer also the possibility to pattern the far field emission and to improve the photon collection efficiency.

For most of these devices, the coupling between the NC and the electromagnetic field depends strongly on the emitter position because of the strong confinement of the plasmon mode. Recently, NCs were integrated into linear gold or silver gratings designed to obtain an enhancement of the fluorescence intensity that is less sensitive to the NC position, especially when NCs are located between the ridges of the grating [18]. Acting as a plasmonic decoupler, the grating opens new radiative decay channels within the line cone in air. This leads to the exaltation of the fluorescence process and the increase of the number of collected photons. The optimization of the grating design enables one to reach an increase by a factor of 3 of the rate of detected photons, regardless of the position of the NC between the ridges.

In this paper, we study the fluorescence properties of the NCs in such a system. The photoluminescence decay rate at the single emitter level is investigated theoretically and experimentally. More specifically, we show that the polarization ratio can exceed 80% while it is lower than 30% when NCs are deposited on a flat gold film. Finally, the autocorrelation function of the intensity for time scales ranging between 10 μs and 100 ms shows that stable emission with Poissonian fluctuations can be achieved.

II. THEORETICAL ANALYSIS

A. Polarization ratio of the emitted signal

1. Individual NC above a flat gold film

The polarization ratio for a single NC placed over a gold film is calculated employing the Fourier modal method following the work of Rigneault and co-workers [19]. The NC emission is modeled with two incoherent dipoles emitting at 660 nm and oriented perpendicular to the NC c axis [20]. The intensity is computed by varying the analyzer direction with respect to the x axis (see Fig. 1). Figure 2 presents the polar plot of the intensity as a function of the analyzer direction for a NC located 15 nm above a flat gold film (thickness of 100 nm). We observe that the emitted signal depends on the NC orientation. In the case of the c axis along z, the emitted signal is not polarized, as expected from symmetry considerations. In the case of the c axis along x, the intensity is slightly polarized along the y axis. Remembering that a NC presenting a c axis aligned with x is modeled by two independent dipoles oscillating along the y and z directions, the intensity polarization is consistent with dipolar scattering perpendicular to the dipole axis but polarized along the dipole axis. This leads to unpolarized light for the z-dipole contribution and y-polarized light for the y-dipole contribution. Similar behavior is observed for a c axis aligned with y.

*jean-pierre.hermier@uvsq.fr

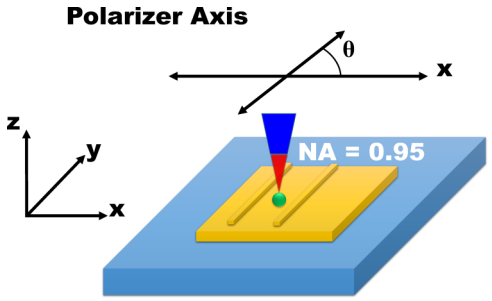

FIG. 1. Polarization measurement of the NC emission. In the plane defined by the gold surface, the x and y axes are respectively orthogonal and parallel to the ridges. θ is the angle between the transmission axis of the linear polarizer and the x axis.

2. *Individual NC on grating decoupler*

Polar plot of the emitted intensity for a NC placed between the ridges of a one-dimensional (1D) grating is calculated as a function of the analyzer angle and presented in Figs. 3(a)–3(c) for the c axis along the x, y, and z directions, respectively (y refers to the invariant direction of the grating). The period of the grating decoupler matches the surface plasmon polariton (SPP) wavelength. We observe a very different behavior as compared to a flat film since the polarization no longer depends on the NC orientation but is fixed by the grating. The emission is now strongly polarized with a polarization along the grating invariant axis (y). More precisely, the polarization ratio of NCs is evaluated as

$$R = \frac{I_{\max} - I_{\min}}{I_{\max} + I_{\min}}, \tag{1}$$

where $I_{\max}$ and $I_{\min}$ are the intensities detected along the maximum pass axis and minimum pass axis. R ranges between 71% [Fig. 3(b), the c axis of the NC along the y axis, 2D dipoles along the x and z axes] and 88% [Fig. 3(a), the c axis oriented along the x axis, 2D dipoles along the y and z axes], with an intermediate value of 78% [Fig. 3(c), the c axis oriented along the z axis, 2D dipoles along the x and y axes].

The orientation of the polarization and these slight variations can be understood by considering the effect of the grating on a 1D dipole emission. The ridges of the grating are oriented along the y axis and support Bloch SPP modes presenting mainly y and z components [originating from the transverse-magnetic (TM)-polarized SPP field propagating along the y axis, and periodic along the x axis]. As a consequence, the x-oriented dipole weakly couples to the grating Bloch modes. On the contrary, the coupling is highest when the 1D dipole is along the y axis. The case of a dipole perpendicular to the surface is intermediate since its emission is isotropic in the xy plane. This analysis also explains why the collected polarization is mainly along the axis of the ridges (y axis).

More generally, R has been evaluated as a function of the c-axis orientation and is presented on a Poincaré sphere in Fig. 4(a) for both NC above a flat film and a 1D grating. The distance to the sphere center is the polarization ratio (that can vary from 0 to 1) and the position on the sphere refers to the c-axis direction. Red points correspond to a NC above a flat gold film. The polarization ratio lies in the range of 0%–20%, and reaches its maximum value for the c axis in the xy plane, as predicted above. Blue points refer to NC into the grating decoupler and R ranges from 70% to 90%. The homogeneous repartition of the points on the sphere reveals that the polarization ratio does not depend on the c-axis orientation.

In the case of grating samples, when the NC is placed near the edge of the nanoridge, the polarization remains along the grating invariant axis but the ratio decreases significantly and reaches values of the order of 20% [the values are presented in Fig. 4(b)].

B. Photoluminescence (PL) decay rate

A 1D grating also significantly modifies the decay rate [18]. To check this, we estimate the total decay rate using Green's dyad formalism (see Refs. [21–23] for details).

Figure 5(a) shows the modification of the 2D local density of states (LDOS) due to the addition of the grating on the flat gold film for a vertically oriented dipole. It presents a resonant behavior, typical from coupling to a mode, here a SPP at an effective index $n_{\mathrm{SPP}} = 1.04$. The bandwidth of the resonance is around 20 nm. Figure 5(b) presents the variation of the total decay rate of a degenerate dipole placed at a height of 15 nm as a function of the position on the 1D grating. The total decay rate value is normalized with respect to the values obtained for NC with the same c-axis orientation placed over the gold film to discuss the experimental results. Figure 5(b) includes the maximum, minimum, and average values of the total decay

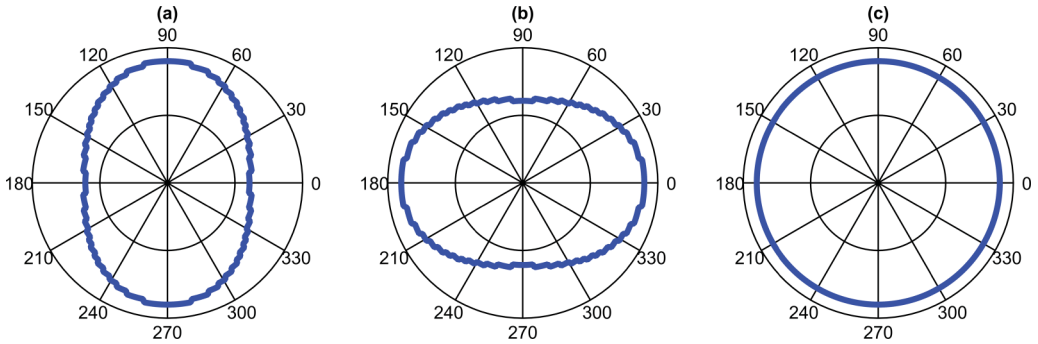

FIG. 2. Polar plot of reflected scattered field of NC emission ($\lambda = 660$ nm) placed at a distance of 15 nm on a thick (100 nm) gold film observed by an analyzer oriented at an angle of θ from the x axis. (a)–(c) are the fields for NC with the c axis along the x, y, and z axes, respectively.

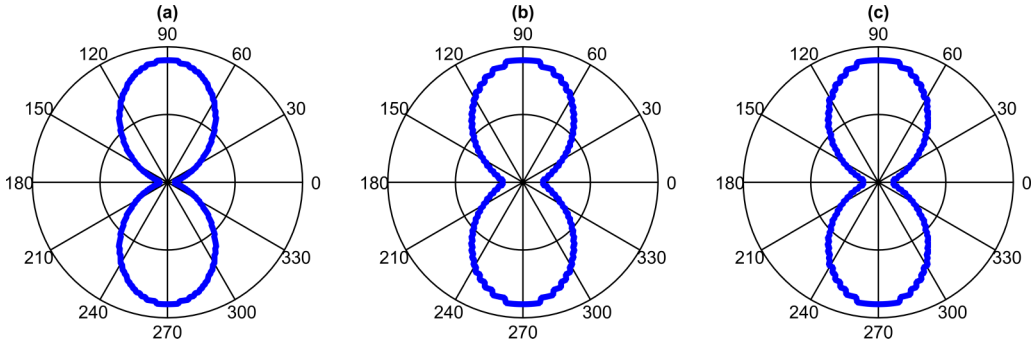

FIG. 3. Polar plot of reflected scattered field of NC emission placed on 1D grating sample (at a distance of 15 nm) observed by an analyzer oriented at an angle of θ from the x axis. (a)–(c) are the fields for NC with the c axis along the x, y, and z axes, respectively.

rate considering the orientation of the 2D dipole. The total decay rate is increased on average for a NC placed over a 1D grating and depends on the NC orientation.

III. EXPERIMENTS

A. Plasmonic grating design

The gold/air SPP effective index for a thick metal film at the emission wavelength of the quantum dot (QD) ($\lambda_{em} = 660$ nm) is $n_{SPP} = k_{SPP}/k_0 = 1.04$ corresponding to the SPP wavelength $\lambda_{SPP} = 635$ nm. Therefore, we fabricated grating decouplers with a period of about $d = 640$ nm. We have first lithographed gold gratings that consist of ten ridges (width $w = 75$ nm, height $h = 100$ nm), above an optically thick gold film (∼100 nm) deposited on an indium tin oxide (ITO) coated glass substrate. Electronic microscope images show that the period typically ranges between 630 and 650 nm.

B. CdSe/CdS nanocrystals

The samples were prepared by spin coating a solution of CdSe/CdS NCs suspended in a mixture of hexane (90%) and octane (10%) on the metallic structures (see Fig. 6). They were synthesized following Ref. [24], having a core of 3-nm radius and a mean shell thickness of 12 nm. The photoluminescence spectrum of a NC ensemble is centered around 660 nm. The full width at half maximum is 33 nm. Considering a homogeneous linewidth of 20 nm [17], this corresponds to an inhomogeneous broadening close to 25 nm. Under air and low excitation power, the intensity fluorescence oscillates between two values corresponding to the recombination of the neutral exciton (X) and trion states (X^*) [25]. As reported recently, CdSe/CdS NCs fluorescence is the incoherent sum of the emission of two linear degenerated orthogonal dipoles [26]. They are 2D dipolar emitters. When deposited on a glass cover slip and characterized by an air objective, the degree of polarization remains always lower than 30%, in agreement with Ref. [26].

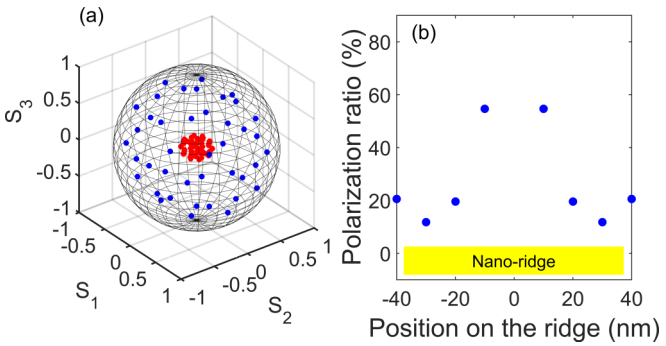

FIG. 4. (a) Polarization ratio simulated for NCs on flat gold films (red squares) and SPP devices (blue circles). The sphere is a reference for the unity polarization ratio. (b) Variation of polarization ratio above the nanoridge showing the smaller values when the NC is close to one edge.

C. Experimental setup

The analysis of the individual NC fluorescence was carried out using a standard confocal microscope setup (the numerical aperture of the objective is 0.95). NCs are optically excited by a pulsed laser diode (wavelength of 405 nm, pulse duration of 100 ps, PicoQuant LDH D-C-405). The fluorescence of the NCs is first detected with a CCD camera that enables one to determine if the NC is located on the flat gold film or on a grating. This microscope is also associated to a Hanbury-Brown and Twiss (HBT) setup. It consists of two avalanche photodiodes (APDs) with a time resolution of 50 ps (PDM series, PicoQuant) connected to a data acquisition card (PicoHarp 300, PicoQuant) that provides the absolute time

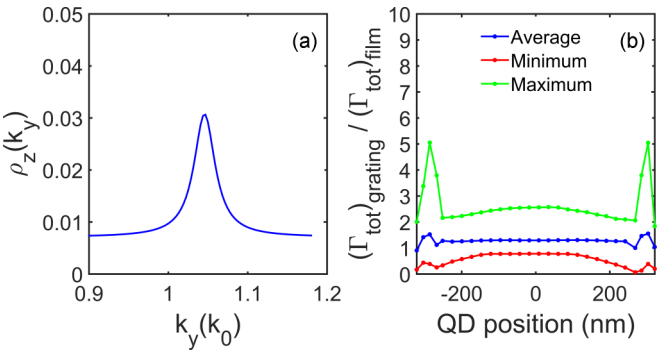

FIG. 5. (a) 2D LDOS calculated inside the 1D grating. LDOS is shown in the range of wave vectors from 0.9 to 1.18 where the dominant peak due to coupling to SPPs is observed. (b) Calculated enhancement in total decay rate as a function of NC position inside the cavity (0 corresponds to the middle between two ridges). Average, minimum, and maximum values are plotted as a function of the orientation of the NC.

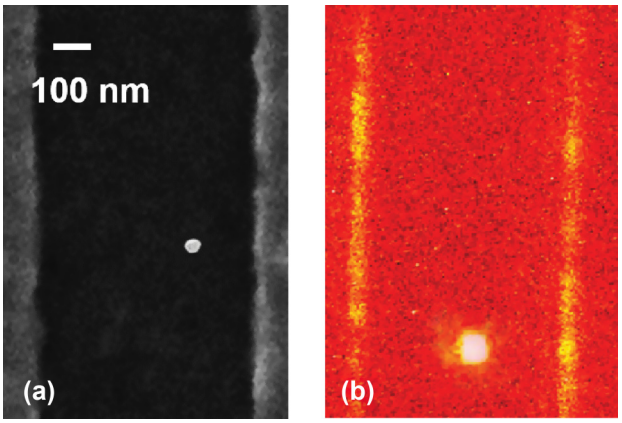

FIG. 6. (a) Scanning electron micrograph image of a NC between two ridges of the grating. (b) Fluorescence of another NC.

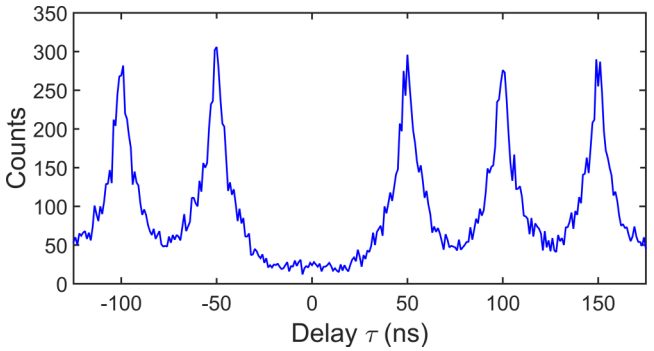

FIG. 7. Coincidence counts corresponding to photons that have been both recorded with a delay greater than 1.5 ns with respect to the pulse laser (method described in Ref. [27]). The NC is located on the gold grating.

of detection of each photon with a time resolution around 128 ps. Each set of data then provides the variation of the intensity with time, the PL decay rate, and the histogram of the coincidences between photons. A rotating polarizer is also placed in front of one of the photodiodes (APD_2). By normalizing the measured intensity by the intensity detected on the other APD, the polarization ratio can be determined precisely even in the case of a small drift of the sample.

IV. FLUORESCENCE PROPERTIES OF A SINGLE NC ON A SPP GRATING

A. Single emitter experiments

NC may form aggregates. In order to prove that the fluorescence of a single nanoemitter is detected, the standard approach consists in measuring photon antibunching using the HBT setup. However, the enhancement of PL decay rate for a NC coupled to a plasmonic resonator results in a strong reduction of the efficiency of the Auger processes. The quantum efficiency of the biexcitonic state is very close to the monoexcitonic one and very low or no antibunching is observed [15]. In this case, Mangum *et al.* [27] showed that a postselection method can be applied with success to suppress the biexcitonic contribution to the autocorrelation function and measure an antibunching amount showing that a single emitter is observed. It consists in keeping only the photons that are detected after a long delay with respect to the NC excitation. Following this method, for several NCs, we calculated the histogram of the delays between the photons detected for delays greater than 1.5 ns after the laser pulse (at these very short delays, the shape of the histogram is not affected by the slow rotation—one revolution per second—of the polarizer located before one of the photodiodes of the HBT setup). The perfect antibunching (see Fig. 7) then observed demonstrates that a single NC emission is characterized.

B. Polarization ratio

Using the HBT setup, the polarization ratio R is now characterized for NCs deposited on the flat gold film and on the 1D gold grating. For the first one [Fig. 8(a)], R is close to or lower than 20%, as expected, except for one NC (27%). The theoretical model shows that this small excess of polarization ratio can come from a larger shell or a lower wavelength emission (data not shown). The position of the polarizer for which the highest value of the intensity is measured is random since it depends only on the orientation of the emitters which are deposited by spin coating. Figure 8(b) shows the results obtained for the 1D grating. R reaches values close or greater than 80% for a majority of the NCs (blue circles), in agreement with the theoretical predictions of Fig. 4. For these emitters, the polarization angle is uniform (its mean value is taken as the reference) and fixed by the grating (we checked that a rotation of 90° of the sample induces a rotation of this angle of the same value). A fraction of the emitters (red squares) exhibit a value of R lower than 50%. As theoretically predicted, such a value of R is expected when the NC is above or close to the edge of a ridge. However, in this case, the polarization angle is fixed by the grating direction. Most of the NCs of which fluorescence is weakly polarized present a polarization angle with an absolute value far from zero. These NCs are thus not well coupled to the 1D grating. Due to the inhomogeneous (∼25 nm) and homogeneous (∼20 nm) linewidths of the NC fluorescence but also the fabrication uncertainty on the period of the grating (leading to a grating resonance uncertainty ∼20 nm), the emission of an individual NC can be partly

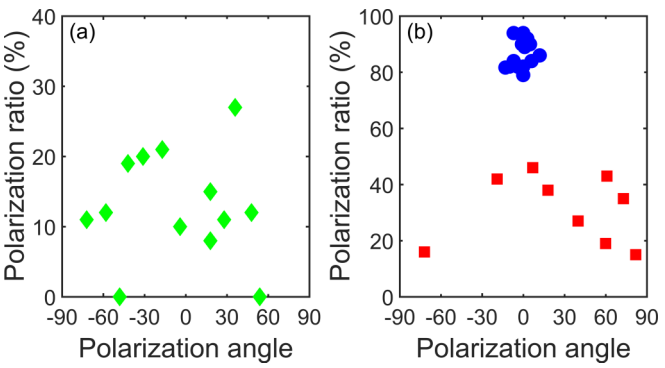

FIG. 8. Polarization ratio and polarization angle measured on individual NCs deposited on the gold film [(a), green diamonds] or on the grating (b). NCs corresponding to blue circles are more efficiently coupled to the grating than the other ones (red squares).

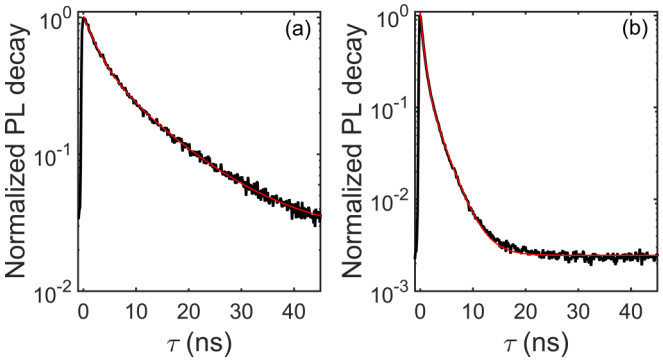

FIG. 9. (a) PL decay of a NC on the flat gold film. The fit (red line) corresponds to the sum of two exponential decays with lifetimes of 2.7 and 12 ns. (b) PL decay of a NC coupled to the grating. The fit (red line) corresponds to the sum of two exponential decays with lifetimes of 0.6 and 2.6 ns.

outside the bandwidth of the grating resonance. Moreover, a large shell or the presence of a thick layer of ligands can act as a spacer and reduce the NC/1D grating coupling. In the following, the NCs which are efficiently coupled to the 1D grating will be referred to as NC* (blue circles).

C. PL decay rate

The modification of the fluorescence of the NCs is now investigated through the PL decay. Figure 9 shows the typical PL decay of one NC deposited on the flat gold film [NC_1, Fig. 9(a)] and on the grating [NC_2, Fig. 9(b)]. In the two cases, the total PL decay is well fitted by a biexponential decay that provides the decay rate of the exciton X (long lifetime) and trion X^* (short lifetime) states [25]. Figure 10(a) represents the polarization ratio R versus the long lifetime component for the NCs considered in Fig. 8. For a NC located 15 nm above the film, the PL decay rate enhancement typically ranges between 0.8 and 2.5 when the grating is used [theoretical predictions of Fig. 5(b)]. This ratio cannot be measured for each NC (the lifetime is measured on the flat film or on the grating). However, the ratio between the mean lifetime of NCs* (blue circles) and the mean lifetime of the NCs deposited on the flat

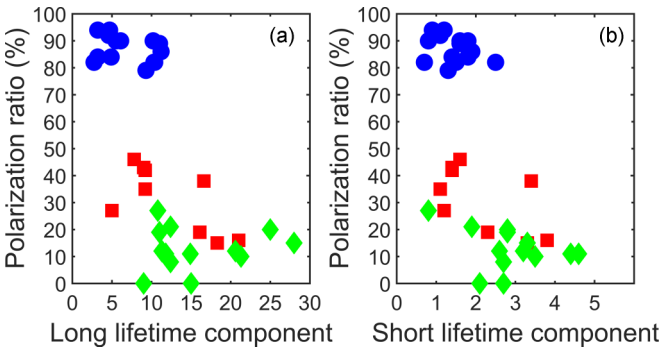

FIG. 10. Polarization ratio as a function of the long lifetime component (a) or short lifetime component (b) of the PL decay. Green diamonds correspond to NCs deposited on the flat gold film, blue circles to NCs efficiently coupled to the grating, and red squares to NCs deposited on the grating but less efficiently coupled.

film (green diamonds) is equal to 2.3, while for the other NCs deposited on the 1D grating (red squares), the corresponding ratio is only equal to 1.3. For the latter, the polarization ratio R, although higher than in the case of the flat gold film, is also lower when compared to NCs*. These consistent results show the low influence of the grating on these NCs' fluorescence (red squares). They appear as only coupled to the metallic film. For the three classes of nanoemitters, one can note a large dispersion of the lifetimes that can be attributed to the random orientation of the 2D dipole but also to the variations of the NC shell thickness, the NC emission, and the grating resonance wavelengths.

The results concerning the long lifetime components are coherent with the ones obtained for the short lifetime component of the X^* state [Fig. 10(b)]. The mean ratio between the long lifetime component (X) and the short one (X^*) is equal to 5.4 for the NCs deposited on the flat gold film and 5.3 for the NCs coupled to the 1D grating. These two values are of the order of magnitude of the one obtained when the NCs are spin coated on a glass cover slip (typically ∼10). Since the resonances of the plasmonic grating are characterized by a broad bandwidth (∼20 nm) when compared to the gap between the X^* and X emission wavelengths (∼5 nm [28]), the Purcell factors for the X and X^* states are close. This observation also confirms the relevancy of measuring the X and X^* state lifetimes with a biexponential fit.

D. Fluorescence blinking

Several experiments [15,24,29,30] have shown that the blinking of colloidal NCs can be suppressed through their coupling with metallic structures. Due to the enhancement of radiative processes, Auger recombination of the X^* becomes negligible and the quantum efficiencies of X and X^* are very close since they are equally coupled to the plasmons.

The blinking modification can be investigated through the autocorrelation function (ACF) of the intensity $g^2(\tau)$. Due to the presence of the rotating polarizer in front of the APD_2, the ACF cannot be calculated from the two photodiodes. Only the data collected by the APD_1 can be used. However, at time scales lower than 10 μs, afterpulsing distorts the signal delivered by the avalanche photodiodes and prevents the correct calculation of the ACF from only one photodiode.

Figure 11 presents the results obtained for two different NCs. The ACF of a NC deposited on the 1D grating [Fig. 11(a)] with a fast PL decay rate remains close to 1 regardless of whether the delays show that blinking is suppressed. For a NC deposited on the flat gold film and exhibiting a slower PL decay [Fig. 11(b)], a small photon bunching corresponding to a residual blinking is observed, but only for delays lower than 10 ms.

V. CONCLUSION

In conclusion, the photoluminescence of thick-shell NCs directly coupled to 1D gold gratings has been investigated in detail. Beyond the enhancement of the PL decay rate of single NCs and the suppression of residual flickering, we showed that the polarization of the emission can be controlled through this system. In the field of quantum plasmonics, our results

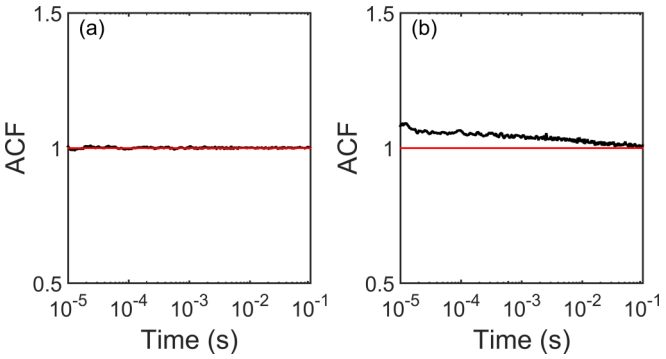

FIG. 11. (a) Normalized area of the peaks of the autocorrelation function ACF of a NC coupled to the gold grating. (b) The same for a NC deposited on a flat gold film.

highlight the interest of associating thick-shell NCs and grating decouplers and could be extended to structures with other symmetries, such as circular ones, to tune the polarization properties of the emission.

ACKNOWLEDGMENTS

This work has been supported by the Agence Nationale de la Recherche (Grant No. QDOTICS ANR-12-BS10-0008). The authors also thank Institut Universitaire de France for funding. Calculations were performed using HPC resources from DSI-CCuB (Université de Bourgogne) and samples were realized using ARCEN nanofabrication facilities.

[1] D. V. Talapin, J. S. Lee, M. V. Kovalenko, and E. V. Shevchenko, Chem. Rev. **110**, 389 (2010).
[2] X. Michalet, F. F. Pinaud, L. A. Bentolila, J. M. Tsay, S. Doose, J. J. Li, G. Sundaresan, A. M. Wu, S. S. Gambhir, and S. Weiss, Science **307**, 538 (2005).
[3] X. Brokmann, E. Giacobino, M. Dahan, and J.-P. Hermier, Appl. Phys. Lett. **85**, 712 (2004).
[4] Y. F. Chen, J. Vela, H. Htoon, J. L. Casson, D. J. Werder, D. A. Bussian, V. I. Klimov, and J. A. Hollingsworth, J. Am. Chem. Soc. **130**, 5026 (2008).
[5] B. Mahler, P. Spinicelli, S. Buil, X. Quélin, J.-P. Hermier, and B. Dubertret, Nat. Mater. **7**, 659 (2008).
[6] F. Cichos, C. Von Borczyskowski, and M. Orrit, Curr. Opin. Colloid Interface Sci. **12**, 272 (2007).
[7] P. A. Frantsuzov, S. Volkán-Kacsó, and B. Jankó, Phys. Rev. Lett. **103**, 207402 (2009).
[8] J. Zhao, G. Nair, B. R. Fisher, and M. G. Bawendi, Phys. Rev. Lett. **104**, 157403 (2010).
[9] J. N. Farahani, D. W. Pohl, H. J. Eisler, and B. Hecht, Phys. Rev. Lett. **95**, 017402 (2005).
[10] J. H. Song, T. Atay, S. Shi, H. Urabe, and A. V. Nurmikko, Nano Lett. **5**, 1557 (2005).
[11] Y. Ito, K. Matsuda, and Y. Kanemitsu, Phys. Rev. B **75**, 033309 (2007).
[12] A. V. Akimov, A. Mukherjee, C. L. Yu, D. E. Chang, A. S. Zibrov, P. R. Hemmer, H. Park, and M. D. Lukin, Nature (London) **450**, 402 (2007).
[13] A. G. Curto, G. Volpe, T. H. Taminiau, M. P. Kreuzer, R. Quidant, and N. F. Van Hulst, Science **329**, 930 (2010).
[14] E. Hwang, I. I. Smolyaninov, and C. C. Davis, Nano Lett. **10**, 813 (2010).
[15] D. Canneson, I. Mallek-Zouari, S. Buil, X. Quélin, C. Javaux, B. Dubertret, and J.-P. Hermier, New J. Phys. **14**, 063035 (2012).
[16] C. Belacel, F. Habert, F. Bigourdan, F. Marquier, J.-P. Hugonin, S. Michaelis de Vasconcellos, X. Lafosse, L. Coolen, C. Schwob, C. Javaux, B. Dubertret, J. J. Greffet, P. Senellart, and A. Maître, Nano Lett. **13**, 1516 (2013).
[17] O. Chen, J. Zhao, V. P. Chauhan, J. Cui, C. Wong, D. K. Harris, H. Wei, H. S. Han, D. Fukumura, R. K. Jain, and M. G. Bawendi, Nat. Mater. **12**, 445 (2013).
[18] A. Kumar, J.-C. Weeber, A. Bouhelier, F. Eloi, S. Buil, X. Quélin, M. Nasilowski, B. Dubertret, J.-P. Hermier, and G. Colas des Francs, Sci. Rep. **5**, 16796 (2015).
[19] H. Rigneault, F. Lemarchand, and A. Sentenac, J. Opt. Soc. Am. A **17**, 1048 (2000).
[20] X. Brokmann, L. Coolen, M. Dahan, and J.-P. Hermier, Phys. Rev. Lett. **93**, 107403 (2004).
[21] J. Barthes, G. Colas des Francs, A. Bouhelier, J.-C. Weeber, and A. Dereux, Phys. Rev. B **84**, 073403 (2011).
[22] J. Barthes, A. Bouhelier, A. Dereux, and G. Colas des Francs, Sci. Rep. **3**, 2734 (2013).
[23] S. Derom, A. Bouhelier, A. Kumar, A. Leray, J.-C. Weeber, S. Buil, X. Quélin, J.-P. Hermier, and G. Colas des Francs, Phys. Rev. B **89**, 035401 (2014).
[24] B. Ji, E. Giovanelli, B. Habert, P. Spinicelli, M. Nasilowski, X. Xu, N. Lequeux, J.-P. Hugonin, F. Marquier, J.-J. Greffet, and B. Dubertret, Nat. Nanotechnol. **10**, 170 (2015).
[25] P. Spinicelli, S. Buil, X. Quélin, B. Mahler, B. Dubertret, and J.-P. Hermier, Phys. Rev. Lett. **102**, 136801 (2009).
[26] C. Lethiec, J. Laverdant, H. Vallon, C. Javaux, B. Dubertret, J.-M. Frigerio, C. Schwob, L. Coolen, and A. Maître, Phys. Rev. X **4**, 021037 (2014).
[27] B. D. Mangum, Y. Ghosh, J. A. Hollingsworth, and H. Htoon, Opt. Express **21**, 7419 (2012).
[28] A. P. Beyler, L. F. Marshall, J. Cui, X. Brokmann, and M. G. Bawendi, Phys. Rev. Lett. **111**, 177401 (2013).
[29] X. W. Wu, M. Gong, C. H. Dong, J. M. Cui, Y. Yang, F. W. Sun, G. C. Guo, and Z. F. Han, Opt. Express **11**, 6340 (2010).
[30] X. Ma, H. Tan, T. Kipp, and A. Mews, Nano Lett. **10**, 4166 (2010).